Time Modulated Antenna Array for Real-Time Adaptation in Wideband Wireless Systems—Part I: Design and Characterization

Grzegorz Bogdan, *Student Member, IEEE,* Konrad Godziszewski, *Member, IEEE,* Yevhen Yashchyshyn, *Senior Member, IEEE,* Cheol Ho Kim, and Seok-Bong Hyun

***Abstract*—This paper presents a design of a time modulated antenna array (TMAA) with substantially wider bandwidth and higher efficiency than have been already presented in the literature. The TMAA is designed for 5.4–5.8 GHz frequency band. More than 50 MHz of channel bandwidth is achieved by utilization of ultra fast microwave switches, digital delay lines with 60 ps step, and fast control circuitry. The efficiency is improved by alternate switching between array elements instead of switching between the array element and a matched load. Moreover, a mathematical derivation of optimal switching sequence is given. The beam-steering at the first sideband frequency was obtained with a 1 degree step in a range from –50 to 50 degrees. The TMAA has been evaluated by means of the radiation pattern measurements at different sideband frequencies.**

***Index Terms*—Adaptive arrays, antennas, antenna arrays, beam–steering, radio frequency (RF) switch, time modulated antenna array, wireless communication.**

I. Introduction

VARIOUS beamforming architectures and algorithms have been invented and implemented to improve performance of wireless communication and radar systems [1]. Typically, beamforming is achieved by a set of antenna weights (amplitude and/or phase) applied to individual elements [2] in digital domain, analog domain, or both (a hybrid approach). Implementation of digital beamforming is challenging due to constraints of cost, power consumption and signal processing complexity. On the other hand, applicability of the phased antenna array (PAA) is limited by the unsatisfactory performance of phase shifters. Therefore, unconventional array architectures and design methodologies have gained a lot of attention over the last two decades [3]. One of the most prospective architectures for a low cost beamforming is based on time-domain processing [4]. The time modulated antenna array (TMAA) is an electromagnetic system whose radiation pattern is controlled by the application of periodical pulses to the individual elements [5]. The TMAA concept is considered as a promising alternative to the PAA because expensive and troublesome phase shifters can be avoided [6]. Output signal of the TMAA is composed of many spectral components (sidebands) at multiples of the modulation frequency around the carrier frequency. This phenomenon used to be considered as a disadvantage. Hence, many techniques for suppression of unwanted sidebands have been proposed [7], [8], [9]. Alternativelly, sidebands can be used to extend capabilities of the TMAA by means of beam-steering [4], [10], [11] and spatial diversity [12], [13].

TABLE I
Overview of TMAA prototypes

f_0	f_c	Switch type	Reference
10 kHz	2.45 GHz	SP4T FET	[15]
10 kHz	5 GHz	RPDC p-i-n diode	[16]
10 kHz	9.375 GHz	SPST p-i-n diode	[17]
10 kHz	36 GHz	surface p-i-n diode	[18]
20 kHz	2.4 GHz	SPDT p-i-n diode	[19]
25 kHz	2.45 GHz	Schottky diode	[20]
100 kHz	1.56 GHz	SPST FET	[21]
100 kHz	2.5 GHz	SP3T	[22]
100 kHz	2.45 GHz	Schottky diode	[23]
100 kHz	2.6 GHz	SPST FET	[24]
100 kHz	3.25 GHz	SPST FET	[25]
125 kHz	9.5 GHz	p-i-n diodes	[26]
1 MHz	2.45/5.8 GHz	SPST p-i-n diode	[27]
1 MHz	2.6 GHz	SPDT FET	[28]
1 MHz	2.525 GHz	SPDT CMOS	[29]
1 MHz	2.525 GHz	SP6T	[30]
1.25 MHz	2.6 GHz	SPST FET	[31]
2.5 MHz	5.8 GHz	SP4T p-i-n diode	[32]
5 MHz	2.6 GHz	SPDT FET	[33]
6.49 MHz	5.8 GHz	SPDT p-i-n diode	[34]
50 MHz	5.6 GHz	SPDT	this work

Many practical TMAAs employing different switching technologies have been designed and evaluated. Performance of curent state–of–the–art TMAAs can be evaluated with the overview of known prototypes presented in Table I. First figure of merit is the bandwidth which usually does not exceed 5 MHz which is below requirements of modern wideband systems. Second crucial parameter is the efficiency. As a matter of fact TMAAs have lower gain than conventional amplitude tapered arrays when the same patterns are synthesized [14], although exact values of the gain or efficiency are usually not reported. Therefore, the main goal of this work was to design and evaluate the TMAA with substantially wider bandwidth and higher efficiency than have been already presented in the

This work was supported by ICT R&D program of MSIP/IITP (2015-0-00268, Development on semi-conductor based smart antenna for future mobile communications).

G. Bogdan, K. Godziszewski and Y. Yashchyshyn are with the Warsaw University of Technology, Institute of Radioelectronics and Multimedia Technology, 00-665 Warsaw, Poland, e-mail: { g.bogdan, k.godziszewski, y.yashchyshyn } @ ire.pw.edu.pl.

C. H. Kim, and S. B. Hyun are with the ETRI (Electronics and Telecommunications Research Institute), 218 Gajeong-ro, Yuseong-gu, Daejeon, 34129, Rep. of Korea, e-mail: { kimcheolho, sbhyun } @ etri.re.kr.

literature. The TMAA presented in this paper provides 7 dBi of realized gain and an outstanding bandwidth of 50 MHz which is sufficient to support transmission of wideband signals in most of current wireless systems.

II. System Fundamental

The TMAA is composed of time modulated elements (TMEs) distributed with uniform spacing and forming a linear array. TMEs are numbered with $n = 0 \dots N-1$. Fig. 1 shows a diagram of the TME cosisting of two oppositely arranged antennas (such element been already proposed in [28]). If a microwave signal $s_n(t)$ is indicent upon the TME perpendicularly, then $s_n(t)$ is received by the upper antenna and $-s_n(t)$ is received by the lower antenna (180° phase difference is due to opposite arrangement of antennas). Next, two signals are delivered to an SPDT microwave switch, which operates alternatively in such a way, that the upper antenna is active for duration τ_n and the lower antenna is active for duration $T_0 - \tau_n$ (the switching is periodical with period T_0). Hence, the output signal $y_n(t)$ is a combination of two signals and has a waveform of a binary phase-keyed signal (similar effect can be achieved by switching between two lines having $\lambda/2$ difference in length [34] or by using two-state phase-shifters [35]). Operation of the TME can be expressed as:

$$y_n(t) = s_n(t) m_n(t) \tag{1}$$

where: $y_n(t)$ is a signal after time modulation, $s_n(t)$ is a single frequency carrier signal, and $m_n(t)$ is a modulating function. Modulating functions are often assumed to be rectangular or trapezoidal due to practical reasons [36]. In our case, to represent operation of the SPDT switch and opposite arrangement of antennas, $m_n(t)$ has a bipolar rectangular waveform with a high value of 1 and a low value of -1 as illustrated in Fig. 3.

The modulating functions can be expressed as a combination of complex Fourier series coefficients $M_n^{(k)}$ [11]:

$$m_n(t) = \sum_{k=-\infty}^{\infty} M_n^{(k)} e^{j2\pi f_0 k t} \quad f_0 = \frac{1}{T_0} \tag{2}$$

$$M_n^{(k)} = \frac{1}{T_0} \int_{-T_0/2}^{T_0/2} m_n(t) e^{-j2\pi f_0 k t} dt \tag{3}$$

where: k – number of the frequency component. Fig. 2 presents Fourier coefficients $M_n^{(k)}$ for a special case of $m_n(t)$ with $\tau_n = T_0/2$. There are two advantages when $\tau_n = T_0/2$. First, it maximizes amplitudes of the first negative ($k = -1$) and the first positive ($k = 1$) sideband components. Second, it doubles spacing between sideband components. Both advantages will be explained in following subsections.

Spectrum of the time modulated signal at the output of each TME can be obtained from:

$$Y_n = S_n * M_n \tag{4}$$

where: $(*)$ denotes the convolution operator and S_n, M_n are sets of Fourier series coefficients of the incident signal and the modulating function, respectively.

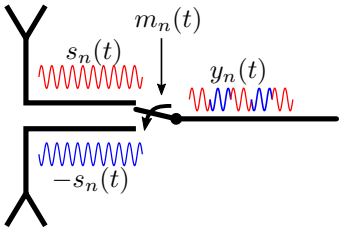

Fig. 1. Diagram of TME

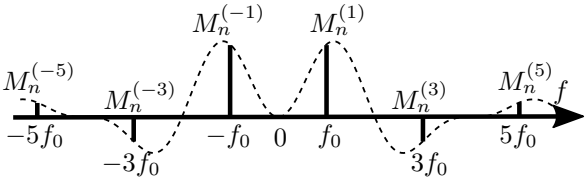

Fig. 2. Spectrum of bipolar modulating function $m_n(t)$ with $\tau_n = T_0/2$ and $\Delta t_n = 0$

A. Single–Sideband Efficieny

Time modulation spreads the power of incident signal to sideband components. Hence, if only one sideband component is used, then the efficiency drops. Shape of the modulating function determines the amplitude and the phase of spectral components. Therefore, appropriate modulating functions should be applied to the array in order to maximize the amplitude of selected sideband component. Fourier series coefficients (3) of bipolar modulating functions, after simple mathematical operations, can be expressed as:

$$M_n^{(k)} = \frac{2\tau_n}{T_0} \operatorname{sinc}\left(k\frac{\tau_n}{T_0}\right) - \operatorname{sinc}(k) \tag{5}$$

where sinc is a normalized sinc function. The highest amplitude for the first negative sideband component ($k = -1$) can be found after taking the derivative of (5) in respect to τ_n:

$$\frac{\partial M_n^{(-1)}}{\partial \tau_n} = \frac{2}{T_0} \cos\left(\frac{\pi\tau_n}{T_0}\right) = 0 \Rightarrow \tau_n = \frac{T_0}{2} \tag{6}$$

Thus, the highest single–sideband efficiency $\eta_{\text{mod}}^{(k)}$ is obtained for equal switching between two antennas of the TME. The single–sideband efficiency can be calculated as the power of the selected sideband component to the total power of the signal, i.e. if $k = -1$ then:

$$\eta_{\text{mod}}^{(-1)} = \frac{\left|Y_n^{(-1)}\right|^2}{\sum_{k=-\infty}^{\infty}\left|Y_n^{(k)}\right|^2} = \frac{\left|M_n^{(-1)}\right|^2}{\sum_{k=-\infty}^{\infty}\left|M_n^{(k)}\right|^2} = 41\% \tag{7}$$

Single–sideband efficiency of proposed TMAA is four times higher than efficiency obtained with absorptive SPST switches with 50% duty cycle. Comparison of single-sideband efficiencies for different methods of time modulation is presented in Table II.

TABLE II
SINGLE–SIDEBAND EFFICIENCIES

	$\eta_{\text{mod}}^{(0)}$	$\eta_{\text{mod}}^{(-1)}$	$\eta_{\text{mod}}^{(-2)}$	$\eta_{\text{mod}}^{(-3)}$
Without time modulation	100%	0%	0%	0%
SPST with 50% duty cycle	25%	10%	0%	1%
SPDT bipolar (this work)	0%	41%	0%	5%

B. Radiation Efficiency

The radiation efficiency (η_{rad}) is defined as the ratio of the total power radiated by an antenna to the net power accepted by the antenna from the connected transmitter [37]. Typically, for a conventional antenna (without time modulation) the radiation efficiency is used to take into account losses at the input terminals and within the structure of the antenna. This includes conduction and dielectric losses (η_{cd}) and losses due to reflections because of the mismatch between the transmission line and the antenna $\eta_r = 1 - |\Gamma|^2$, where Γ is the voltage reflection coefficient at the input terminals of the antenna [2]. In case of the TMAA three additional factors should be considered:

- the reflection losses caused by the impedance mismatch between transmission lines and ports of the RF switch,
- the efficiency of RF switches which can be defined as $\eta_{\text{sw}} = 1/L_{\text{sw}}$, where ($L_{\text{sw}}$ is the insertion loss given in linear scale),
- the efficiency drop caused by absorptive switches when turned off (η_{OFF}).

After consideration of all aforementioned factors the radiation efficiency of the TMAA can be written as:

$$\eta_{\text{rad}} = \eta_r \eta_{cd} \eta_{\text{sw}} \eta_{\text{OFF}} \tag{8}$$

Efficiency calculations for the designed antenna are presented in section IV-C.

C. Maximum Signal Bandwidth

Typically, modulation frequency should be greater than the bandwidth of a linearly-modulated digital signal to avoid overlapping of spectral replicas [38]. However, the TMAA proposed in this paper can be used to transmit signals exceeding this limitation. This is possible because the center frequency component and the evenly numbered sideband components are not present.

The center frequency component ($k = 0$) is not present because the 180° phase shift due to opposite arrangement of patches is not compensated with a phase shift due to the time modulation. This phenomenon occurs only if an incident wave is perpendicular to the TME. Otherwise, the center frequency component will not be completely canceled, but suppressed dependently on the incident angle.

Spectral components of even orders are not present, because the sinc function has nulls in these points:

$$M_n^{(k)} = \text{sinc}\left(\frac{k}{2}\right) - \text{sinc}(k) = 0 \quad \text{if} \quad k = 0, \pm 2, \pm 4, \ldots \tag{9}$$

Therefore, only odd sideband components ($k = \pm 1, \pm 3, \pm 5, \ldots$) exist, which doubles the bandwidth.

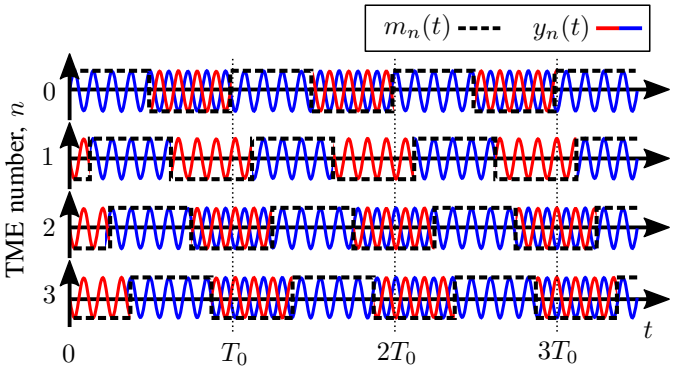

Fig. 3. Modulated signals and progressively delayed modulating functions

D. Beam-steering

Let us now consider a TMAA composed of $N = 4$ linearly and uniformly distributed TMEs, where modulating functions are bipolar square waveforms with $\tau_n = T_0/2, \forall\, n = 0 \ldots N-1$ and are delayed by Δt_n in respect to the first modulating function $m_0(t)$ ($\Delta t_0 = 0$). Fig. 3 presents an example of such modulating functions. Output $f(t)$ from the array is a superposition of the time modulated signals $y_n(t)$ from all TMEs:

$$f(t) = \sum_{n=0}^{N-1} y_n(t) = \sum_{n=0}^{N-1} s_n(t) m_n(t) \xrightarrow{\mathfrak{F}} F = \sum_{n=0}^{N-1} S_n * M_n \tag{10}$$

Phase-control can be applied to the modulating functions on the basis of a well known time-shift property of the Fourier series which states, that the time–delay Δt_n in the time domain causes the phase shift in the frequency domain:

$$m_n(t) = m_0(t - \Delta t_n) \Rightarrow M_n^{(k)} = M_0^{(k)} e^{-j2\pi k \Delta t_n / T_0} \tag{11}$$

Therefore, delays of modulating functions Δt_n cause the phase shift similar to a conventional phased array. For example, if $T_0 = 20$ ns and $\Delta t_n = 0.056$ ns, then -1° phase phase-shift on the first negative sideband component is achieved. Beam-steering can be achieved by the phase-progression on sideband components due to delay-progression of modulating functions $\Delta t = \Delta t_{n+1} - \Delta t_n$, i.e. delay of modulating functions for consecutive TMEs is increased by Δt in respect to the preceding TME:

$$m_n(t) = m_0(t - n\Delta t) \tag{12}$$

Hence, the first negative sideband component of the output signal of the beam-steering TMAA can be expressed as:

$$\begin{aligned} F^{(-1)} &= M_0^{(-1)} \sum_{n=0}^{N-1} S_n e^{j2\pi \Delta t_n / T_0} \\ &= M_0^{(-1)} \sum_{n=0}^{N-1} S_n e^{j2\pi n \Delta t / T_0} \end{aligned} \tag{13}$$

III. Proposed TMAA System

The TMAA forms a system which includes an antenna array with switches, an antenna controller, and an adaptive algorithm. Schematic of the system is presented in Fig. 4. The design, principles of operation, and microwave measurements are described in this section. Adaptive algorithm and study of adaptation are presented in the second part of this paper [39].

A. Antenna Array with RF switches

The TME shown in Fig. 1 was implemented as a structure composed of two oppositely oriented aperture-coupled series-fed patches. This TMAA design has been already proposed [28]. However, it is now improved with a second patch to increase the gain and to narrow the main beam in the E-plane (YZ-plane). Patch antennas are formed on a superstrate above the ground plane and are electromagnetically coupled with feeding network through a small apertures (slots in the ground plane). Aperture-coupled design is particularly advantageous when applied to TMAAs because the ground plane shields the antenna from spurious radiation emitted by feedlines and microwave switches. Moreover, with the two-layer design, patches are located on a lower permittivity substrate ($\varepsilon_r = 2.2$), which provides wide impedance bandwidth and high radiation efficiency, whereas the feeding network lays on a higher permittivity substrate ($\varepsilon_r = 3.66$) which yields lower radiation losses [40].

Four TMEs were used to form an antenna array with beam-steering capability in the H-plane (XZ-plane). The antenna was fabricated in a multilayer printed circuit board (PCB) technology. The top layer with patch antennas is presented in Fig. 5a and the bottom layer with switches is presented in Fig. 5b. Fig. 5a shows also the radiation pattern of a 30° beam simulated in an electromagnetic (EM) computer software.

RF switches are critical elements of the time modulation circuitry. The RF rise/fall time of the switch determines the maximum bandwidth of a signal which can be transmitted/received by the TMAA without overlapping of spectral replicas. In order to achieve wideband operation very short switching time $t_{\mathrm{RF}}^{\mathrm{sw}} < 5$ ns from 10% to 90% RF is necessary. In addition to timing parameters also microwave parameters have to be considered, i.e. insertion loss (L_{sw}), and reflection loss ($|\Gamma|$). Comparison of high-performance switches is presented in Table III. Switch ADRF5020 [41] was selected based on ultra short switching time ($t_{\mathrm{RF}}^{\mathrm{sw}} = 2$ ns) and very good microwave performance at 5.6 GHz. It is worth mentioning that ultra fast switches with $t_{\mathrm{RF}}^{\mathrm{sw}} < 0.1$ ns operating in mm-wave have been already presented in the literature [42] and hopefully will be available commercially for further improvement of the TMAA performance.

B. Antenna Controller

The antenna controller changes states of RF switches in required timing. It should provide a high pulse repetition frequency and a variable delay of control signals. The controller proposed in this work is similar to the one presented in [34], although in our case much higher modulation frequency

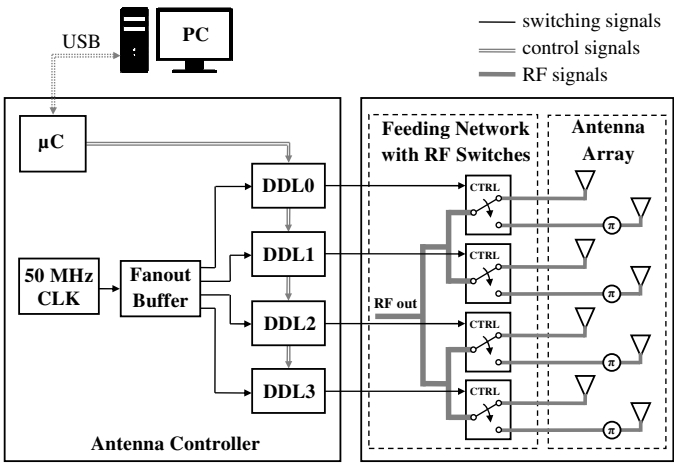

Fig. 4. Schematic of TMAA

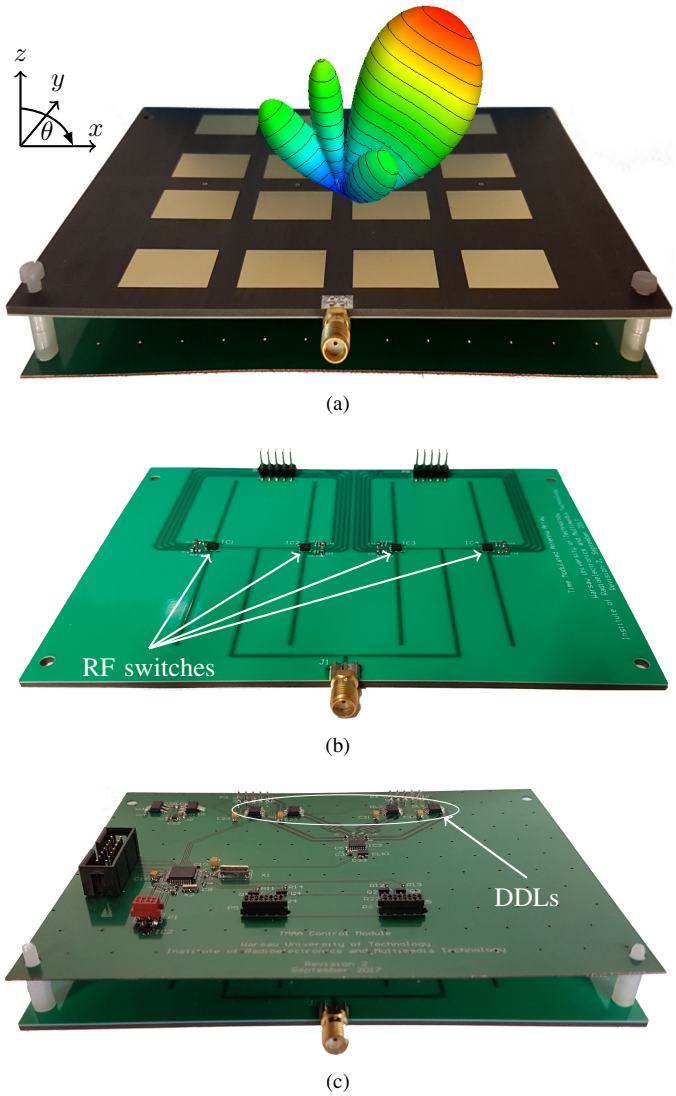

(a)

(b)

(c)

Fig. 5. Fabricated TMAA (a) top layer with patch antennas and simulated 3D pattern of 30° beam (b) bottom layer with feeding network and switches (c) control board

TABLE III
COMPARISON OF SPDT SWITCHES

Ref	L_{sw} (dB)	$\|\Gamma\|$ (dB)	t_{RF}^{sw} (ns)	B (GHz)	P_{max} (dBm)	Technology
[43]	0.5	−20	20	DC–20	33	Si p-i-n
[44]	2.0	−10	3	DC–8	27	GaAs MESFET
[45]	1.7	−17	2	DC–20	30	GaAs pHEMT
[41]	1.2	−22	2	DC–30	27	Si
[42]	1.3	−5	0.03	42–70	1	SiGe HBT

was obtained. Its schematic and picture after fabrication are presented in Fig. 4 and Fig. 5c, respectively. The design is straightforward thanks to the LVTTL/CMOS driver built in the RF switch [41]. Moreover, due to 50% duty cycle of all modulating functions, a commercial 50 MHz MEMS clock signal generator with high stability of ±10 ppm could be used (the controller has been also tested with higher frequencies of the clock signal generator, i.e.: 80 MHz, 100 MHz and 125 MHz). Delays are applied with 8-bit programmable digital delay lines (DDLs) with a fine step of 60 ps and a maximum value of 15.3 ns [46]. Fig. 6 and Table IV give examples of DDL settings directing the beam for $k = -1$ toward angle θ_{max}^{-1}. For example, if $\theta_{max}^{-1} = -45°$ is required, then $\Delta t = -0.441T_0$. Thus, for $T_0 = 50$ MHz, $\Delta t_0 = 0$ ns, $\Delta t_1 = -8.82$ ns, $\Delta t_2 = -17.64$ ns, and $\Delta t_3 = -26.46$ ns. Next, due to periodicity of modulating functions, we can add 20 ns to both the second and the third delays, hence $\Delta t_2 = 2.36$ ns and $\Delta t_3 = -6.46$ ns. Negative delays are not possible to apply, therefore a constant value of 8.82 ns is added to all delays in order to obtain positive values without loosing the relative relations: $\Delta t_0 = 8.82$ ns, $\Delta t_1 = 0$ ns, $\Delta t_2 = 11.18$ ns, and $\Delta t_3 = 2.36$ ns. Then, the values are divided by the step of 60 ps to obtain register values: DDL0 = 147, DDL1 = 0, DDL2 = 187, DDL3 = 40.

Each DLL is programmed independently from a personal computer (PC) via universal serial bus (USB), which is used also as a power supply for all active components. A microcontroller is used to receive data from the PC and to set delays on four daisy-chained DDLs.

IV. CHARACTERIZATION OF DESIGNED TMAA

A. Switching

Parameters of the selected switch were measured on a test board with a sampling oscilloscope. Measured output signal is presented in Fig. 7. The RF rise time from 10% to 90% of the maximum amplitude is around 1.5 ns. The duty cycle measured between 50% of the rising edge and 50% of the falling edge is close to a half of the modulation period $T_0/2 = 10$ ns.

B. Bandwidth

Fig. 8 shows measured spectrum of a signal at the output of the TMAA when illuminated from broadside direction $\theta = 0°$ with a continuous wave signal with $f_c = 5.6$ GHz (without progressive delay, i.e. $\Delta t = 0$). Settings of the measurement are gathered in Table V. Levels of the center frequency component and evenly ordered components are respectively 25 dB

TABLE IV
SETTINGS OF DDLS

DDL0	DDL1	DDL2	DDL3	$\Delta t/T_0$	Δt (ns)	θ_{max}^{-1}
147	0	187	40	−0.441	−8.82	−45°
198	132	66	0	−0.198	−3.96	−20°
0	0	0	0	0	0	0°
0	66	132	198	0.198	3.96	20°
40	187	0	147	0.441	8.82	45°

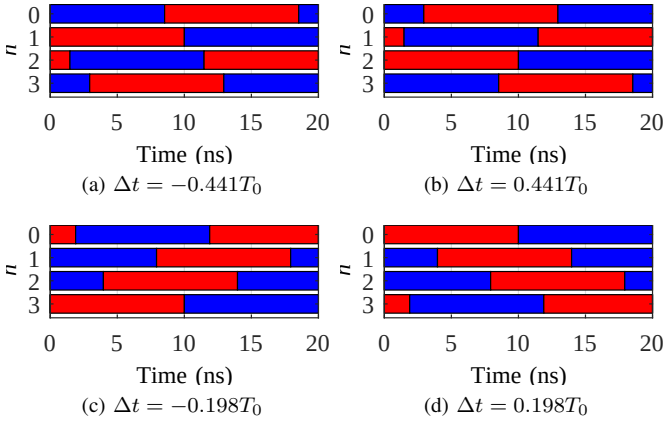

(a) $\Delta t = -0.441T_0$ (b) $\Delta t = 0.441T_0$
(c) $\Delta t = -0.198T_0$ (d) $\Delta t = 0.198T_0$

Fig. 6. Examples of switching sequences (blue and red colors represent switching between two antennas in TME)

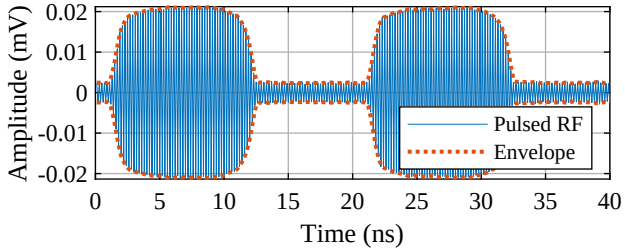

Fig. 7. Output of RF switch

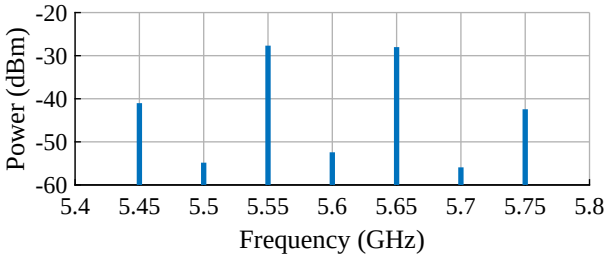

Fig. 8. Measured spectrum of TMAA output signal

TABLE V
SETTINGS OF SPECTRUM ANALYZER

Parameter	Setting
Center frequency	5.6 GHz
Frequency span	500 MHz
Number of points	101
Resolution bandwidth	1 MHz
Detector type	Sampling detector

and 27 dB lower than level of the first sideband component. Therefore, if $f_0 = 50$ MHz it is possible in some conditions to transmit a signal with a maximum bandwidth of 100 MHz, because degradation of the SNR due to overlaping of spectral replicas will be negligible.

C. Efficiency and Gain

The radiation efficiency (η_r) of designed TMAA can be calculated according to (8) after consideration of following partial efficiencies:

- $\eta_{\text{OFF}} = 1$, because proposed architecture does not dissipate power in off-state,
- $\eta_r \approx 1$, thanks to negligibly low impedance mismatch between microstrip lines, patch antennas, and switches,
- $\eta_{cd} = 0.8$, due to efficient design of the antenna array (the value was computed using an EM simulator),
- $\eta_{\text{sw}} = 1/1.32 = 0.76$, because insertion loss of the RF switch $L_{\text{sw}} = 1.2$ dB (1.32 in linear scale).

Hence, $\eta_{\text{rad}} = 0.6$. The TMAA system efficiency which includes all RF losses and efficiency of the first negative sideband component equals:

$$\eta_{\text{TMAA}}^{(-1)} = \eta_{\text{rad}}\eta_{\text{mod}}^{(-1)} = 0.6 \cdot 0.41 \approx 0.25 \tag{14}$$

In order to calculate the TMAA gain both the directivity and the efficiency should be considered. The directivity $D = 16.5$ dBi was obtained from EM simulations. However, the simulations were performed for a static excitation of all array elements. In case of the proposed TMAA only half of elements is active, therefore the aperture efficiency $\eta_a = 0.5$. Eventually, calculated TMAA gain at the first negative sideband component equals:

$$G_{\text{TMAA}}^{(-1)} = D\eta_{\text{TMAA}}^{(-1)}\eta_a = 7.4 \text{ dBi} \tag{15}$$

Calculations were confirmed by means of measurements for $k = \{-1, 0, +1\}$ and variable carrier frequency f_c. Obtained values of the TMAA gain are presented in Fig. 9.

D. Radiation Patterns and Beam-steering

Radiation patterns of antennas are typically obtained from measurements of the transmission coefficient acquired with the vector network analyzer (VNA). However, in case of the TMAA the transmitting and the receiving frequencies may differ. In consequence it is not possible to directly measure

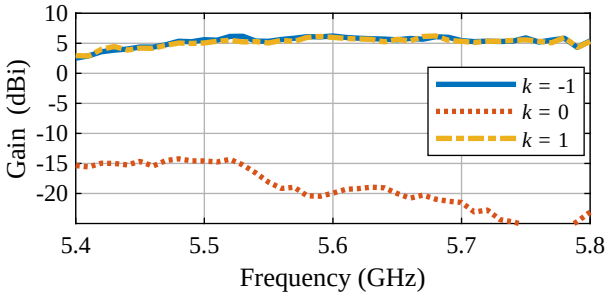

Fig. 9. Measured gain of TMAA

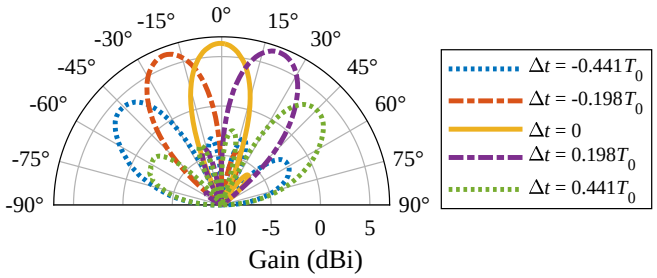

Fig. 10. Radiation patterns in H-plane measured at $k = -1$ for different Δt

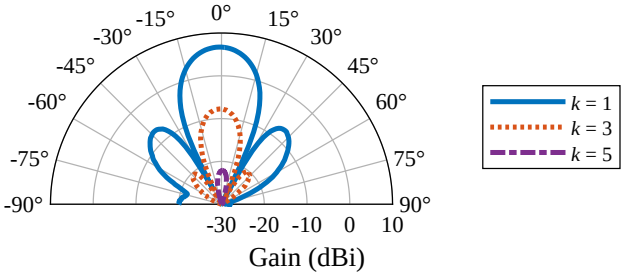

Fig. 11. Measured radiation patterns in H-plane for $\Delta t = 0$

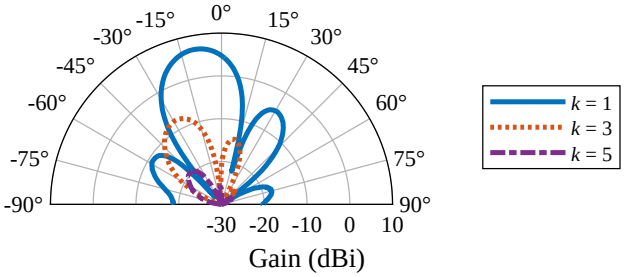

Fig. 12. Measured radiation patterns in H-plane for $\Delta t = 0.1T_0$

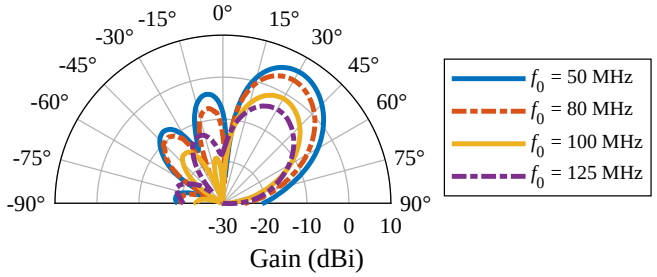

Fig. 13. Radiation patterns of 15° beam measured for various modulation frequencies

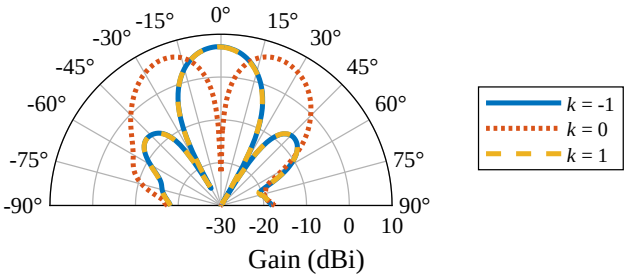

Fig. 14. Radiation patterns in E-plane

the TMAA pattern [47], therefore a procedure based on a microwave signal generator and a spectrum analyzer was used [48]. A total number of 121 beams steered from -60° to 60° with 1° step was measured. Selected radiation patterns measured in the H-plane at $k = -1$ for delays gathered in Table IV are presented in Fig. 10. The highest TMAA gain $G_{\text{TMAA}}^{(-1)} = 7$ dBi was measured for 0° beam. In this case the half–power beam–width HPBW $= 24^\circ$ and the sidelobe level SSL $= 14$ dB. The gain drops when increasing the scanning angle, reaching $G_{\text{TMAA}}^{(-1)} = 3.5$ dBi for 50° beam. For wider scanning angles the sidelobe level increases. Therefore, satisfactory scanning sector is 100° wide. The set of measured beams was used to implement an adaptive antenna system which is described in the second part of this paper [39].

Radiation patterns measured at sideband components $k = \{1, 3, 5\}$ without steering ($\Delta t = 0$) are presented in Fig. 11. Radiation patterns have almost identical shape, however different gains. The gain drops more than 10 dB for $k = 3$ and more than 25 dB for $k = 5$ which corresponds with measurements of spectrum (Fig. 8). Fig. 12 shows radiation patterns measured at the same sideband frequencies as presented in Fig. 11, although with $\Delta t = 0.1T_0$.

Radiation patterns measured at sidebands components of higher orders are steered toward larger angles proportionally to its order. Such diversity of beams can be used for multichannel spatial transmission. Radiation patterns measured for various frequencies of time modulation $f_0 \in \{50, 80, 100, 125\}$ MHz are presented in Fig. 13. If the time modulation frequency increases, then the duration of transient between two states of the RF switch become more significant in relation to the modulation period. The highest gain was achieved for $f_0 = 50$ MHz. Faster control of the RF switch leads to a decrease of the gain. On the other hand, higher f_0 enables transmission of signals with wider bandwidth. Therefore, a satisfactory trade-off between the gain and the system bandwidth should be found when applying the TMAA into a wireless system.

According to the spectral analysis presented in Fig. 8 the radiation pattern at the center frequency ($k = 0$) has a deep null in a broadside direction. This was confirmed by radiation pattern measurements in the E-plane (non-scanning plane) presented in Fig. 14. The gain at the center frequency is less than 0 dBi for the angular sector of 10°. Therefore, the center component may limit the maximum bandwidth of signals if they are arriving from diverse directions, especially in multipath environments.

V. Conclusion

Improvement of the TMAA efficiency was achieved by means of alternative switching between pair of elements connected to an SPDT switch. In addition, proposed method of time modulation avoided generation of evenly numbered sideband components, which led to a wider bandwidth.

An outstanding bandwidth of 50 MHz was achieved as a result of a very short switching time of state–of–the–art RF switches applied in presented design of the TMAA. In addition, a specially designed controller based on a MEMS clock signal generator and programmable semiconductor delay lines with a 60 ps delay step was used to perform beam-steering with a 1° resolution. Good efficiency, wide bandwidth and beam-steering capability of the TMAA prove its high potential as an adaptive antenna for wireless communication devices.

References

[1] R. A. Monzingo, R. L. Haupt, and T. W. Miller, *Introduction to Adaptive Arrays*. Scitech Publishing, 2011.
[2] C. A. Balanis, *Antenna theory: analysis and design*. John Wiley & Sons, 2012.
[3] P. Rocca, G. Oliveri, R. J. Mailloux, and A. Massa, "Unconventional phased array architectures and design methodologies - a review," *Proc. IEEE*, vol. 104, no. 3, pp. 544–560, Mar. 2016.
[4] H. Shanks, "A new technique for electronic scanning," *IRE Trans. Antennas Propag.*, vol. 9, no. 2, pp. 162–166, Mar. 1961.
[5] R. Maneiro-Catoira, J. Brégains, J. A. García-Naya, and L. Castedo, "Time modulated arrays: from their origin to their utilization in wireless communication systems," *Sensors*, vol. 17, no. 3, p. 590, Mar. 2017.
[6] Y. Yashchyshyn, K. Godziszewski, G. Bogdan, and P. Piasecki, "X-band antenna array for low-cost beam scanning," *IET Microw. Antennas Propag.*, vol. 11, no. 15, pp. 2174–2178, Dec. 2017.
[7] S. Yang, Y. B. Gan, and A. Qing, "Sideband suppression in time-modulated linear arrays by the differential evolution algorithm," *IEEE Antennas Wireless Propag. Lett.*, vol. 1, pp. 173–175, 2002.
[8] D. Gwak, I. Sohn, and S. H. Lee, "Analysis of single-RF MIMO receiver with beam-switching antenna," *ETRI Journal*, vol. 37, no. 4, pp. 647–656, Aug. 2015.
[9] T. D. Drysdale, B. Allen, and E. Okon, "Sinusoidal time-modulated uniform circular array for generating orbital angular momentum modes," in *11th Eur. Conf. Antennas Propag. (EuCAP)*, Paris, France, Mar. 2017, pp. 973–977.
[10] C. He, L. Wang, J. Chen, and R. Jin, "Time-modulated arrays: A four-dimensional antenna array controlled by switches," *Journal of Communications and Information Networks*, vol. 3, no. 1, pp. 1–14, Mar. 2018.
[11] L. Poli, P. Rocca, G. Oliveri, and A. Massa, "Harmonic beamforming in time-modulated linear arrays," *IEEE Trans. Antennas Propag.*, vol. 59, no. 7, pp. 2538–2545, Jul. 2011.
[12] P. Rocca, Q. Zhu, E. Bekele, S. Yang, and A. Massa, "4-D arrays as enabling technology for cognitive radio systems," *IEEE Trans. Antennas Propag.*, vol. 62, no. 3, pp. 1102–1116, Nov. 2014.
[13] R. Maneiro-Catoira, J. C. Brégains, J. A. García-Naya, L. Castedo, P. Rocca, and L. Poli, "Performance analysis of time-modulated arrays for the angle diversity reception of digital linear modulated signals," *IEEE J. Sel. Topics Signal Process.*, vol. 11, no. 2, pp. 247–258, Mar. 2017.
[14] Q. Zhu, S. Yang, R. Yao, and Z. Nie, "Gain improvement in time-modulated linear arrays using SPDT switches," *IEEE Antennas Wireless Propag. Lett.*, vol. 11, pp. 994–997, 2012.
[15] G. Bogdan, P. Bajurko, and Y. Yashchyshyn, "Null-steering in two-element time modulated linear antenna array through pulse-delay approach," in *20th Int. Conf. Microw. Radar Wireless Commun. (MIKON)*, Gdańsk, Poland, Jun. 2014, pp. 1–4.
[16] J. Chen, X. Liang, C. He, H. Fan, W. Zhu, R. Jin, and J. Geng, "Efficiency improvement of time modulated array with reconfigurable power divider/combiner," *IEEE Trans. Antennas Propag.*, vol. 65, no. 8, pp. 4027–4037, Aug. 2017.
[17] W. Kummer, A. Villeneuve, T. Fong, and F. Terrio, "Ultra-low sidelobes from time-modulated arrays," *IEEE Trans. Antennas Propag.*, vol. 11, no. 6, pp. 633–639, Dec. 1963.
[18] Y. Yashchyshyn, K. Derzakowski, P. Bajurko, J. Marczewski, and S. Kozłowski, "Time–modulated reconfigurable antenna based on integrated S–PIN diodes for mm–wave communication systems," *IEEE Trans. Antennas Propag.*, vol. 63, no. 9, pp. 4121–4131, Sep. 2015.
[19] A. Tennant, "Experimental two-element time-modulated direction finding array," *IEEE Trans. Antennas Propag.*, vol. 58, no. 3, pp. 986–988, Mar. 2010.
[20] D. Masotti, A. Costanzo, M. D. Prete, and V. Rizzoli, "Time-modulation of linear arrays for real-time reconfigurable wireless power transmission," *IEEE Trans. Microw. Theory Techn.*, vol. 64, no. 2, pp. 331–342, Feb. 2016.

[21] S. Yang, Y. B. Gan, A. Qing, and P. K. Tan, "Design of a uniform amplitude time modulated linear array with optimized time sequences," *IEEE Trans. Antennas Propag.*, vol. 53, no. 7, pp. 2337–2339, Dec. 2005.

[22] A. M. Yao, W. Wu, and D. G. Fang, "Study on reconfigurable coaperture antenna arrays based on time-modulation and retrodirective techniques," *IEEE Trans. Antennas Propag.*, vol. 64, no. 5, pp. 1713–1724, May 2016.

[23] P. Rocca, D. Masotti, A. Costanzo, M. Salucci, and L. Poli, "The role of accurate dynamic analysis for evaluating time-modulated arrays performance," *IEEE Antennas Wireless Propag. Lett.*, vol. 16, pp. 2663–2666, 2017.

[24] Q. Zhu, S. Yang, R. Yao, M. Huang, and Z. Nie, "Unified time- and frequency-domain study on time-modulated arrays," *IEEE Trans. Antennas Propag.*, vol. 61, no. 6, pp. 3069–3076, Jun. 2013.

[25] Q. Zhu, S. Yang, L. Zheng, and Z. Nie, "Design of a low sidelobe time modulated linear array with uniform amplitude and sub-sectional optimized time steps," *IEEE Trans. Antennas Propag.*, vol. 60, no. 9, pp. 4436–4439, Sep. 2012.

[26] Y. Wang and A. Tennant, "Experimental time-modulated reflector array," *IEEE Trans. Antennas Propag.*, vol. 62, no. 12, pp. 6533–6536, Dec. 2014.

[27] R. Gahley and B. Basu, "A time modulated printed dipole antenna array for beam steering application," *Int. J. Antennas Propag.*, Feb. 2017.

[28] G. Bogdan, Y. Yashchyshyn, and M. Jarzynka, "Time-modulated antenna array with lossless switching network," *IEEE Antennas Wireless Propag. Lett.*, vol. 15, pp. 1827–1830, 2016.

[29] C. He, X. Liang, Z. Li, J. Geng, and R. Jin, "Direction finding by time-modulated array with harmonic characteristic analysis," *IEEE Antennas Wireless Propag. Lett.*, vol. 14, pp. 642–645, 2015.

[30] C. He, X. Liang, B. Zhou, J. Geng, and R. Jin, "Space-Division Multiple Access Based on Time-Modulated Array," *IEEE Antennas Wireless Propag. Lett.*, vol. 14, pp. 610–613, 2015.

[31] C. He, X. Liang, W. Zhu, G. Geng, R. Jin, A. Cao, and H. Di, "Direction finding by time modulated linear array," in *Proc. IEEE Int. Symp. Antennas and Propag. USNC/URSI National Radio Science Meeting*, San Diego, California, USA, Jul. 2017, pp. 315–316.

[32] J. D. Fredrick, Y. Wang, and T. Itoh, "A smart antenna receiver array using a single RF channel and digital beamforming," *IEEE Trans. Microw. Theory Techn.*, vol. 50, no. 12, pp. 3052–3058, Dec. 2002.

[33] G. Jo, J. N. Lee, H. O. Bae, Y. H. Lee, D. Gwak, and J. H. Oh, "LTE based spatial multiplexing MIMO with single radio," in *46th Eur. Microw. Conf. (EuMC)*, London, UK, Oct. 2016, pp. 1319–1322.

[34] S. Farzaneh and A. R. Sebak, "Microwave sampling beamformer - prototype verification and switch design," *IEEE Trans. Microw. Theory Techn.*, vol. 57, no. 1, pp. 36–44, Jan. 2009.

[35] A.-M. Yao, W. Wu, and D.-G. Fang, "Single-Sideband Time-Modulated Phased Array," *IEEE Trans. Antennas Propag.*, vol. 63, no. 5, pp. 1957–1968, May 2015.

[36] E. T. Bekele, L. Poli, P. Rocca, M. D'Urso, and A. Massa, "Pulse-shaping strategy for time modulated arrays–analysis and design," *IEEE Trans. Antennas Propag.*, vol. 61, no. 7, pp. 3525–3537, 2013.

[37] *Standard for Definitions of Terms for Antennas*, IEEE 145-1993 Std., 2014.

[38] R. Maneiro-Catoira, J. C. Brégains, J. A. García-Naya, and L. Castedo, "On the feasibility of time-modulated arrays for digital linear modulations: A theoretical analysis," *IEEE Trans. Antennas Propag.*, vol. 62, no. 12, pp. 6114–6122, Dec. 2014.

[39] G. Bogdan, K. Godziszewski, and Y. Yashchyshyn, "Time modulated antenna array for real-time adaptive beamforming in wideband wireless systems–part 2: Adaptation study," *IEEE Trans. Antennas Propag., unpublished*, 2019.

[40] P. Sullivan and D. Schaubert, "Analysis of an aperture coupled microstrip antenna," *IEEE Trans. Antennas Propag.*, vol. 34, no. 8, pp. 977–984, Aug. 1986.

[41] *ADRF5020 - 100 MHz to 30 GHz, silicon SPDT switch*, Analog Devices, Dec. 2017. [Online]. Available: http://www.analog.com/media/en/technical-documentation/data-sheets/ADRF5020.pdf

[42] M. Thian and V. F. Fusco, "Ultrafast Low–Loss 42–70 GHz Differential SPDT Switch in 0.35um SiGe Technology," *IEEE Trans. Microw. Theory Techn.*, vol. 60, no. 3, pp. 655–659, 2012.

[43] *MASW-00x100 Series HMIC silicon PIN diode switches*, Macom, Jun. 2018. [Online]. Available: https://cdn.macom.com/datasheets/MASW-00x100.pdf

[44] *HMC347C8 - GaAs MMIC SMT high isolation SPDT switch, DC - 8 GHz*, Analog Devices, Jun. 2018. [Online]. Available: http://www.analog.com/media/en/technical-documentation/data-sheets/hmc347c8.pdf

[45] *HMC547ALP3E - GaAs MMIC SPDT non-reflective switch, DC - 20 GHz*, Analog Devices, 2018. [Online]. Available: http://www.analog.com/media/en/technical-documentation/data-sheets/HMC547ALP3E.pdf

[46] *Monolithic 8-bit programmable delay line (series 3d3438)*, Data Delay Devices, Dec. 2017. [Online]. Available: http://www.datadelay.com/datasheets/3d3438.pdf

[47] S. Farzaneh, A. K. Ozturk, A. R. Sebak, and R. Paknys, "Antenna-pattern measurement using spectrum analyzer for systems with frequency translation," *IEEE Antennas Propag. Mag.*, vol. 51, no. 3, pp. 126–131, Jun. 2009.

[48] G. Bogdan, K. Godziszewski, and Y. Yashchyshyn, "Feasibility of standard instrumentation for radiation pattern measurement of time modulated antenna array," in *22nd Int. Microw. Radar Conf. (MIKON)*, Poznań, Poland, Jun. 2018, pp. 420–423.

Grzegorz Bogdan (S'16) was born in Poland in 1989. He received the B.E. degree in electrical and computer engineering and the M.E. degree in telecommunications from Warsaw University of Technology (WUT), Warsaw, Poland, in 2012 and 2013, respectively. In 2013 he was an exchange student at University of Waterloo, Canada. Since 2016 he has been with the Institute of Radioelectronics and Multimedia Technology, WUT, where he is currently working toward the Ph.D. degree. His research interests include reconfigurable antenna arrays, time modulation, and wireless communications.

Konrad Godziszewski (S'12–M'17) was born in Warsaw, Poland, in 1986. He received the M.E. degree in electronics and telecommunications in 2011, and the Ph.D. in telecommunications in 2018, both from Warsaw University of Technology (WUT), Warsaw, Poland. He joined the Institute of Radioelectronics and Multimedia Technology, WUT, in 2013 where he is currently an Assistant Professor. He has authored or coauthored over 50 technical papers. His current research interests include antennas, material characterization in sub-terahertz frequency range, and ferroelectric materials.

Yevhen Yashchyshyn (M'96–SM'09) received the M.E. degree from Lviv Polytechnic National University, Lviv, Ukraine, in 1979, the Ph.D. degree from Moscow Institute of Electronics and Mathematics (MIEM), Moscow, Russia, in 1986, and the D.Sc. (Habilitation) degree from Warsaw University of Technology (WUT), Warsaw, Poland, in 2006. In 2016 he was promoted to a Professor Title. Since 1999 he has been with the Institute of Radioelectronics and Multimedia Technology, WUT, where he is currently a Professor and a Deputy Director for Research. He has authored over 250 technical papers, authored or co-authored 5 books, and holds a few patents. His current research interests include antenna theory and techniques, smart beamforming, reconfigurable antennas, radio over fiber techniques, and materials characterization, including ferroelectric ceramic-polymers composites investigation up to subterahertz frequency. Prof. Yashchyshyn was the recipient of the First Prize of EuMA at the 11th European Microwave Week for his outstanding research and new concept of the reconfigurable antenna, Amsterdam, the Netherlands, 2008.

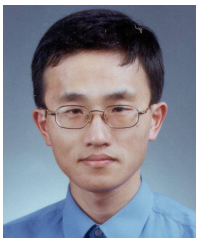

Seok-Bong Hyun received the BS, MS, and PhD degrees in applied physics from the Korea Advanced Institute of Science and Technology (KAIST) in 1991, 1993, and 1998, respectively. In 1999 he joined Electronics and Telecommunications Research Institute (ETRI), Korea, where he has been involved in the design of RF and analog integrated circuits for short-range wireless communication systems and semiconductor-based beamforming antenna. His research interests include the design of mixed signal IC and millimeter wave radio for 5G and beyond network.

Cheol Ho Kim received the BC, MS, and Ph.D. degrees in electrical engineering from Korea Institute of Science and Technology (KAIST), Daejeon, in 2004, 2006, and 2012, respectively.

He is currently a senior research engineer at Electronics and Telecommunication Research Institute (ETRI), Korea. He has broad research interests including wireless communication systems, monolithic microwave integrated circuits, power amplifiers, machine learning, and artificial intelligence (AI). He is currently focusing on developing a new machine learning algorithms for cognitive AI.